



Effect of heat exchanger design on seasonal performance of heat pump systems

Shehryar Ishaque^a, Md Irfanul Haque Siddiqui^b, Man-Hoe Kim^{a,*}

^aSchool of Mechanical Engineering & IEDT, Kyungpook National University, Daegu 41566, South Korea

^bDepartment of Mechanical Engineering, King Saud University, Riyadh, Saudi Arabia

ARTICLE INFO

Article history:

Received 29 October 2019

Revised 1 January 2020

Accepted 18 January 2020

Keywords:

Heat exchanger design

CFD

Face velocity profile

Heat pump

Seasonal performance

ABSTRACT

This paper presents the effect of heat exchanger design on heat pump performance based on partial load operating conditions. 3-D numerical analysis was conducted to calculate face velocity profiles for each outdoor heat exchanger design (rectangular, cylindrical, and trapezoidal) in 10 different operating conditions. Heat exchanger circuits were modified considering heat exchanger face velocity distributions, and seasonal heat pump performances were calculated with modified heat exchanger design. The maximum seasonal performance enhancement of 7.07% was achieved with a modified heat exchanger design. Air-side flow maldistribution could affect significantly refrigerant path design and heat exchanger performance as well as system performance. The analysis results also revealed that smaller refrigerant circuits at the upper part of the heat exchanger interacting with higher air velocity could further enhance the annual system performance.

© 2020 Elsevier Ltd. All rights reserved.

1. Introduction

Energy and environmental issues are critical problems due to rapid increases in energy systems around the world. The International Energy Agency has reported that energy systems such as air conditioning and heat pump systems account for almost 700 million metric tons of CO₂ equivalent direct (7%–19%) and indirect emissions (74%) per year, which is responsible for global warming and ozone depletion. Direct emissions can be reduced by introducing low global warming potential (GWP) refrigerants, and indirect emissions can be controlled using a more efficient system [1].

The finned tube heat exchanger is widely used as a condenser or evaporator of heat pump systems, and it is one of the most important components of the systems and plays a significant role in the system size and performance. Therefore, it is important to design more efficient, lightweight, cost-effective, and low power consuming finned tube heat exchangers [2,3].

Heat exchanger performance degradations are associated with maldistribution of refrigerant and face air velocity distribution, particularly for downstream rows as airflow velocity decreases significantly on the lower side [4]. Although it is difficult to measure the air velocity profile experimentally [5], it strongly influences heat exchanger performance [6]. Non-uniform flow distribution has

many disadvantages: produces wake in flow [7], changes flow pattern [8], decreases overall heat transfer coefficient [9], and reduces system capacity [10]. Consequently, it also increases pressure drop [11] across the heat exchanger hence increases required pumping power [12–15]. Performance deterioration due to non-uniform flow is not limited to finned tube heat exchangers with louver fins [9] and plate fins [16,17], but also occurs in concentric tube [14], and microchannel condensers of automotive air conditioning systems [18]. These examples highlighted the problem of non-uniform flow distribution in different applications. However, these studies are limited to rated load conditions for specific heat exchanger design. No study has been found in literature that covers face velocity distribution for outdoor heat exchanger under partial load operating conditions. Therefore, it is important to evaluate face velocity profiles under off-design condition.

Many techniques have been used by researchers to improve flow distribution uniformity. Recently Saeed and Kim [19] proposed to replace the zigzag pathway for printed circuit heat exchanger by smooth sinusoidal path to reduce non-uniformity and hence improve performance. Similarly, employing V- rather than A-shaped air-cooled condensers [20], adjusting condenser coil included angle [21], inclining heat exchanger relative to fan or increasing plenum depth [22], optimized header design [23], and triangular-shaped air guide plates [24] can also improve uniformity and hence enhance heat exchanger performance. Although proposed modifications in literature are effective but limited to heat exchanger coil adjustment with respect to flow velocity. However, airflow profiles

* Corresponding author.

E-mail address: manhoe.kim@knu.ac.kr (M.-H. Kim).

Nomenclature

A	surface area, m^2
C_p	specific heat capacity, kJ/kg
COP	coefficient of performance
EER	energy efficiency ratio
ε	heat exchanger effectiveness
$elbu$	required capacity of an electric backup heater, kW
F_i	fraction of total refrigerant mass flow rate flowing through i^{th} circuit
G_i	refrigerant mass flux for i^{th} circuitry branch, kg/m^2s
h	heat transfer coefficient, W/m^2K
H	the number of hours the unit is considered to work in
H_{ce}	equivalent cooling hours
K_p	thermal conductivity of the tube, $W/m K$
m	mass flow rate, kg/s
Pr	Prandtl number
P	the electricity consumption, kW
$P_{design,c}$	full load electricity consumption, kW
Q	heat transfer rate or reference annual demand, kW or kWh
R	flow resistance offered by a given branch leaving a split
SEER	seasonal energy efficiency ratio
SCOP	seasonal coefficient of performance
TOL	Temperature operating limit
T	temperature, $^{\circ}C$ or K
T_j	corresponding temperature or bin temperature, K
U	overall heat transfer coefficient or turbulent velocity, W/m^2K or m/s
u_{max}	maximum velocity, m/s
X_p	thickness of the tube wall, m
<i>Greek symbols</i>	
Φ	fin efficiency
ω	humidity ratio, $(kg_w/kg_{a,dry})$
α	$i_{fgw} (\omega_a - \omega_w) / (C_{pa}(T_a - T_w))$
μ	dynamic viscosity, Ns/m^2
<i>Subscript</i>	
a	air-side
c	cooling
CK	crankcase heater mode
f	fin
h	heating
i	inner side of the tube, inlet or i^{th}
j	the bin number
l	liquid or latent
m	mean
max	maximum
n	the amount of bins
o	outer side of the tube
OFF	OFF mode
r	refrigerant side
SB	standby mode
t	tube
TO	thermostat off mode
w	wall tube or water

Assuming uniform refrigerant or airflow is not recommended for most numerical models or optimization techniques as it has a significant effect on system performance results [25–29]. There are $n!$ possible circuits for a heat exchanger with n tubes [30] and the connections can be W-, U-, or Z-shaped. A more uniform temperature distribution has been achieved with Z-shaped connections where the concentrated mass flow area interacted with high-temperature zones [31]. Although this improves heat transfer performance, the pumping power requirements also increase due to longer circuits. Therefore, smaller refrigerant circuits are required to reduce pumping power without compromising on heat transfer in any operating conditions.

The literature review suggests that various techniques have been developed in the past to improve air and refrigerant flow uniformity for system performance enhancement. However, these techniques are limited to specific designs under rated load conditions which results in high energy consumption throughout the year, especially in non-peak operating conditions. The heat pump performance analysis based on partial load operating conditions has not been carried out in literature to the best of the author's knowledge. Therefore, the present study proposes an energy-efficient heat pump system under partial load operating conditions. Cycle simulation is performed for 3 different outdoor heat exchanger configurations. Face velocity profiles have been calculated using computational fluid dynamics for 10 different cooling/heating conditions and used as an input to the cycle simulation. The thermo-hydraulic performance of the heat pump system is evaluated in terms of seasonal energy efficiency ratio (SEER) and seasonal coefficient of performance (SCOP).

2. Methodology

2.1. System description

Fig. 1 shows the heat pump system considered in this study comprised of four basic components: compressor, indoor heat exchanger, expansion device, and outdoor heat exchanger. Outdoor and indoor heat exchangers are both finned tube heat exchangers comprising a bundle of tubes connected in different patterns through which refrigerant flows. Each tube is a single tube cross-flow heat exchanger subjected to a specific portion of airflow. Three outdoor unit heat exchanger shapes were investigated: rectangular, cylindrical, and trapezoid as shown in Fig. 2. All other geometric and operating parameters were kept constant for each design. Table 1 shows the simple system specifications.

2.2. CFD modeling

Several models have been proposed in the past to predict airflow based on the assumption of uniform distribution which can lead to significantly inaccurate results [32]. Domanski and Yashar [33] emphasized finding the non-uniform flow distribution to evaluate finned tube heat exchanger performance.

Fig. 2 shows the three heat exchanger shapes considered in the current study. Each heat exchanger consists of 180 staggered tube arrays with louvered wide fins. Solving the flow profile through the heat exchanger directly with any finite arithmetic is time-consuming and requires prohibitively high computational efforts. Therefore, the current heat exchanger has been modeled as a porous medium which is numerically an efficient way to calculate the face velocity profiles for an outdoor unit heat exchanger [34]. It reduces simulation complexities and time requirements without compromising on the accuracy of the results. A porous medium approach is used in a variety of applications such as tube banks, per-

changes with outdoor operating condition. Hence, it is necessary to modify the shape of the heat exchanger rather than inclining coils in order to reduce non-uniformity in each operating condition.

Maldistribution of airflow distribution causes uneven refrigerant mass flow which further deteriorates heat exchanger performance.

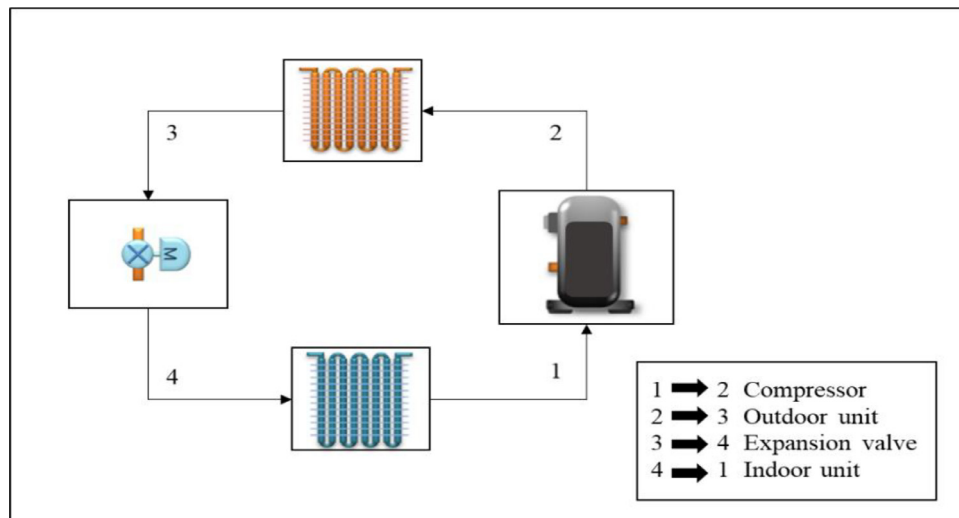


Fig. 1. Simplified system description.

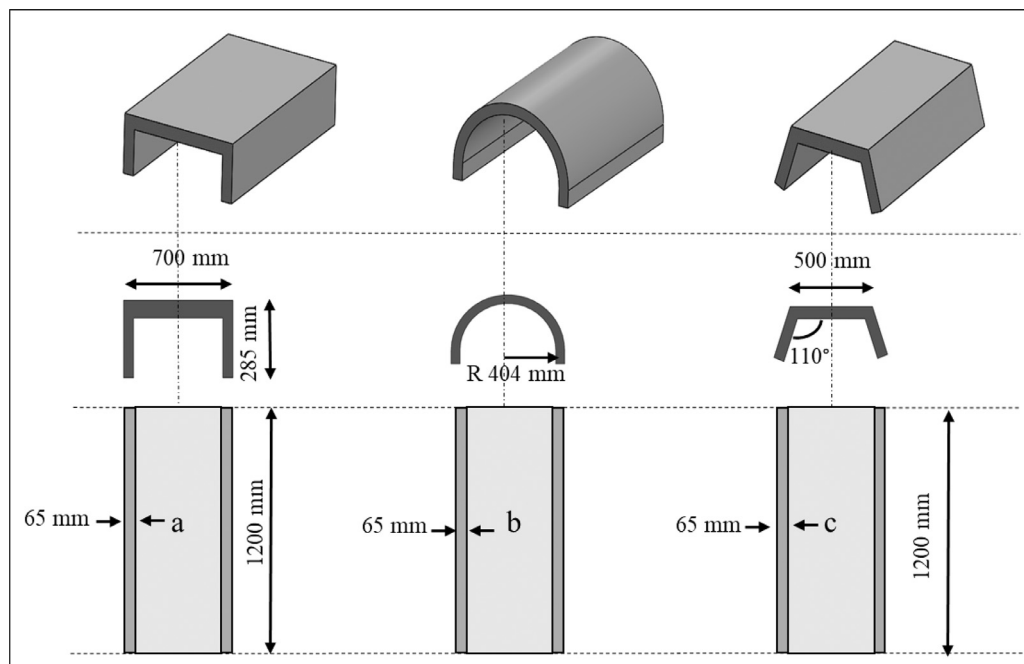


Fig. 2. Heat exchanger configurations (a) rectangular, (b) cylindrical and (c) trapezoidal.

Table 1
System specifications.

Item	Specification
Refrigerant/oil	R410A/POE
Compressor	Scroll compressor
Indoor heat exchanger	Tube diameter $\phi = 7.0$ mm, 3 rows, 56 steps, 168 tubes, 1040 mm total length
Outdoor heat exchanger	Tube diameter $\phi = 7.0$ mm, 3 rows, 60 steps, 180 tubes, 1720 mm total length
Expansion device	Capillary ($\phi = 4.76$ mm, total length = 240 mm)
Fin type and pitch (Indoor/outdoor)	Slit 1.5 mm/Louver 1.7 mm

forated plates, filter papers and flow distributors [35]. An and Kim [36] used a simple porous medium approach to calculate face velocity distribution of the cross flow heat exchanger with test data for velocity and pressure-drop.

Fig. 3 shows a simple outdoor unit and corresponding computational domain for the heat exchanger and fluid flow zones.

We then solved the governing equations for three dimensional (3-D) steady incompressible flow using the CFD code [35]: mass

conservation,

$$\frac{\partial \rho}{\partial t} + \nabla \cdot (\rho \vec{v}) = 0, \quad (1)$$

and momentum conservation,

$$\frac{\partial}{\partial t} (\rho \vec{v}) + \nabla \cdot (\rho \vec{v} \vec{v}) = -\nabla p + \nabla \cdot (\bar{\tau}) + \rho \vec{g} + F, \quad (2)$$

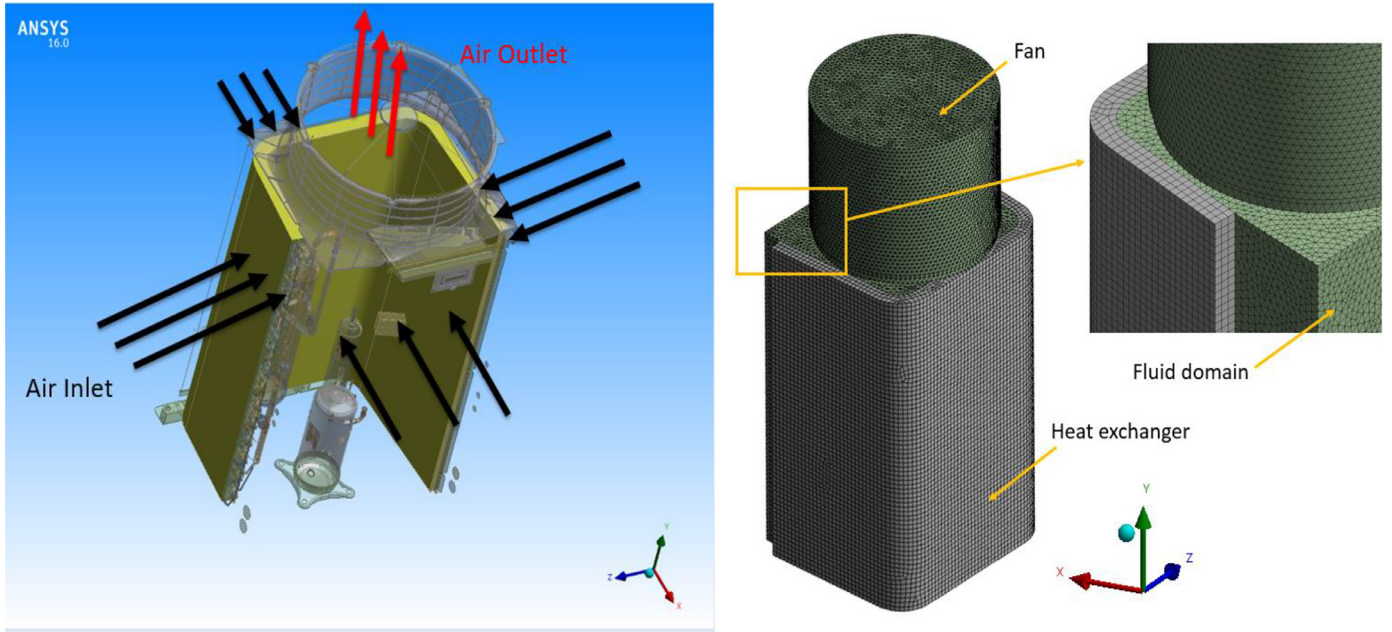


Fig. 3. Simplified outdoor unit with discretized porous medium and fluid flow zones.

where p is static pressure, v is velocity, ρ is density, $\rho \vec{g}$ and F are gravitational and external body forces, respectively, including the source term for porous media; and $\bar{\tau}$ is the stress tensor,

$$\bar{\tau} = \mu \left[(\nabla \vec{v} + \nabla \vec{v}^T) - \frac{2}{3} \nabla \cdot \vec{v} I \right] \quad (3)$$

where μ is the molecular viscosity, and I is the unit tensor.

The standard k - ε turbulence model was utilized to resolving turbulence in the fluid domain, the simplest two-equation turbulence model in which the solution of two separate transport equations allows turbulent velocity and length scales to be independently determined,

$$\frac{\partial}{\partial t} (\rho K) + \text{div}(\rho K U) = \text{div} \left[\left(\frac{\mu_t}{\sigma_k} \right) \text{grad } K \right] + 2\mu_t S_{ij} \cdot S_{ij} - \rho \varepsilon, \quad (4)$$

where K is the turbulent kinetic energy, U is the turbulent velocity, μ_t is eddy viscosity, S_{ij} represents a component of the rate of deformation.

Thus, the dissipation rate for turbulent kinetic energy ε can be expressed as

$$\frac{\partial}{\partial t} (\rho \varepsilon) + \text{div}(\rho \varepsilon U) = \text{div} \left[\left(\frac{\mu_t}{\sigma_\varepsilon} \right) \text{grad } \varepsilon \right] + C_{1\varepsilon} \frac{\varepsilon}{K} 2\mu_t S_{ij} \cdot S_{ij} - C_{2\varepsilon} \rho \frac{\varepsilon^2}{K}, \quad (5)$$

and turbulent eddy viscosity is derived by combining K and ε ,

$$\mu_t = \rho C_\mu \frac{K^2}{\varepsilon}, \quad (6)$$

where C_μ is a dimensionless constant. For turbulent flows, the following values [37] were adopted for the constants: $C_{1\varepsilon} = 1.44$, $C_{2\varepsilon} = 1.92$, $C_\mu = 0.09$, $\sigma_k = 1$, and $\sigma_\varepsilon = 1.30$.

Reynolds stresses were calculated from the Boussinesq relationship [38],

$$-\rho \overline{u_i u_j} = \mu_t \left(\frac{\partial U_i}{\partial x_j} + \frac{\partial U_j}{\partial x_i} \right) - \frac{2}{3} \rho k \delta_{ij} = 2\mu_t S_{ij} - \frac{2}{3} \rho k \delta_{ij}. \quad (7)$$

The flow was assumed laminar in the porous medium and the standard k - ε turbulence model was used to resolve turbulence in

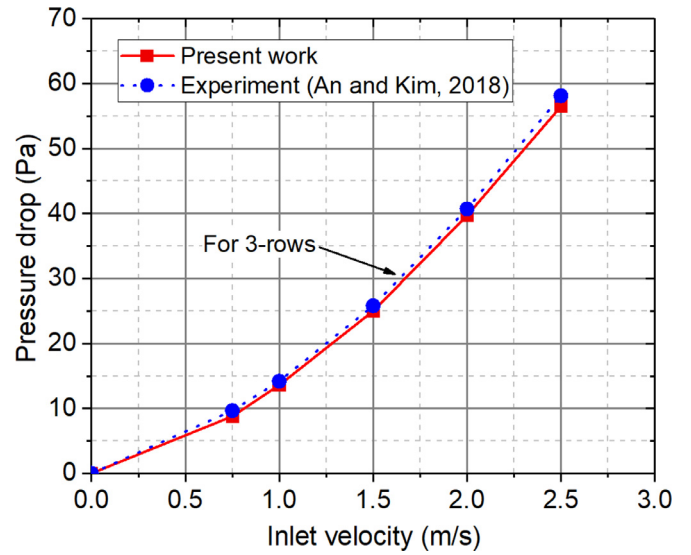


Fig. 4. CFD model validation using An and Kim [36] test data.

fluid flow zones. Upstream and downstream boundaries were kept sufficiently far from the heat exchanger, and no-slip conditions prescribed at the solid wall. Domain elements were optimized for accurate and computationally efficient modeling.

Table 2 compares the results obtained from different number of grids. Pressure drops approximately 4.43% from Mesh 2 to Mesh 3. Further grid refinement reduced this difference to approximately 1.31%. Similar results were found for face velocity. Thus, Mesh 3 was selected for optimal accuracy and computational efficiency. Fig. 3 shows the discretized heat exchanger and fluid flow domains. We created a hexahedral mesh for the porous media domain (heat exchanger), and the fluid flow zone has meshed with fine tetrahedral elements. Numerical results were compared with the published data by An and Kim [36]. Fig. 4 shows pressure drop with respect to inlet velocity, confirming that numerical results were in good agreement with experimental results, within 2.14% even at higher velocities.

Table 2
Grid independency test.

Mesh	Number of grids	Face velocity difference (%)	Pressure drop difference (%)	CPU time per iteration (s)
Mesh 1	815,611	6.1	7.12	74
Mesh 2	1,552,816	3.8	4.43	122
Mesh 3	1,822,544	2.4	1.31	169
Mesh 4	2,286,923	2.4	1.31	232

2.3. Heat transfer calculations

The finned tube heat exchanger model can be solved through tube by tube or section by section methods [39]. The current program uses the tube by tube method, where outlets from the first tube are considered as inputs to the second tube, etc. Parametric tube details; inlet conditions, properties, and mass flow rates for air and refrigerant are known parameters and provide input for the first tube. Heat transfer from air to refrigerant can be expressed as

$$Q_a = m_a c_{pa} (T_{ai} - T_{ri}) \varepsilon, \quad (8)$$

where Q_a is the air-side heat transfer rate, m_a is the air mass flow rate, c_{pa} is the specific heat of the air, T_{ai} is the airside inlet temperature, T_{ri} is the refrigerant side inlet temperature, ε is the heat exchanger effectiveness.

The overall heat transfer coefficient U is the sum of five serial resistances: convective air resistance, conductive resistance as heat transferred through the tube wall, contact resistance through water layer in case of wet conditions, a contact resistance between outside tube wall and fin collar, convective resistance of the refrigerant. If there is a water layer on the fin and tube surface, then conduction resistance through that water layer will also be involved,

$$U = \left(\frac{A_o}{h_i A_{pi}} + \frac{A_o X_p}{A_{pm} K_p} + \frac{1}{h_i} + \frac{A_o}{A_{po} h_{pf}} + \frac{1}{h_o (1 + \alpha) \left(1 - \frac{A_f}{A_o} (1 - \phi) \right)} \right)^{-1}, \quad (9)$$

where U is the overall heat transfer coefficient, A_o is outside surface area exposed to air, A_f is fin surface area, A_{pi} is tube inside surface area, A_{pm} is mean surface area, A_{po} is tube outside surface area, h_i is inside tube heat transfer coefficient, h_{pf} thermal conductance of the pipe-to-fin contact, h_l is convection heat transfer coefficient through water layer, h_o is convection heat transfer coefficient on air-side, X_p is tube thickness, K_p is tube thermal conductivity, and $\phi = \frac{T_{fm} - T_a}{T_{fb} - T_a}$; fin efficiency, T_a is air temperature, T_{fm} is fin mean temperature, and T_{fb} is fin base temperature.

After calculating U from Eq. (9), tube wall and fin's surface temperatures can be calculated using heat transfer resistances. Finned tube heat exchangers can have several numbers of circuits, so the total mass flow rate of refrigerant will be divided among the circuits such that total pressure drop across the heat exchanger remains the same. Thus, the fraction of refrigerant through each circuit can be expressed as Eq. (10) [39]

$$F_i = \frac{m_i}{m_{tot}} = \frac{1}{\sum_{j=first}^{last} (R_i/R_j)^{0.571}}, \quad (10)$$

where $R_i = \Delta P_i / \Delta G_i^{1.75}$ is total refrigerant flowing through the i -th circuit, $R_j = \Delta P_j / \Delta G_j^{1.75}$ is total flow resistance for all branches splitting from that point. The first iteration loop estimates R_i . Resistance in each tube is assumed to be the same regardless of flow quality. Therefore, initial R_i depends on the number of refrigerant

circuits and their paths. Subsequent iterations update R_i and F_i values. Iteration continues until the pressure drop across each circuit becomes uniform.

Heat transfer and pressure drop correlations for different fin types have been widely disseminated previously. Thus, friction factor f and colburn j factor equations for the current fin-type under consideration can be expressed as Eqs. (11) and (12) respectively [40].

$$f = \frac{2 A_{min} \Delta P}{\rho A_i u_{max}^2} \quad (11)$$

Where A_{min} is the minimum flow area, A_i its surface area exposed to air, ρ is the air density and u_{max} is the maximum velocity.

$$j = \frac{\eta_s h_{co} Pr^{2/3}}{\rho u_{max} c_{pa}} \quad (12)$$

where η_s is the surface efficiency, h_{co} is convection heat transfer coefficient at the exterior surface, Pr is the Prandtl number, c_{pa} is the specific heat capacity of air-side.

2.4. Energy efficiency ratio and coefficient of performance

The basic vapor compression cycle was implemented in the cycle simulation program [41] to calculate EER or COP for cooling and heating modes respectively. It included indoor and outdoor unit finned tube heat exchanger models that act as condensers or evaporators depending on the operating mode. Finned tube heat exchangers are the main components of the cycle, and are solved using the tube-by-tube method. Non-uniform air flow velocity distribution was used as an input to the heat exchanger along with other parameters given in Table 1. Each tube is a single tube cross flow heat exchanger subjected to a specific amount of air flow. Once heat exchanger capacity and evaporator or condenser outlet conditions are evaluated, the refrigerant saturation temperatures are used to solve the thermodynamic cycle. The software uses a built-in compressor map data for the selected type of compressor which adjusts refrigerant flow rate and compressor power. Compressor isentropic efficiency and volume flow rate were calculated for the specified saturation temperatures at compressor inlet and outlet. Energy efficiency ratio or coefficient of performance is calculated using heat exchanger capacity divided by total power input, including the power required by fan of the corresponding heat exchanger.

2.5. Seasonal energy efficiency ratio and seasonal coefficient of performance

Heat pumps are generally designed for a peak load condition, however this is not an ideal or efficient way to design heat pump, as the system will only operate at these conditions 1–2.5% per year [42]. Therefore, SEER and SCOP are expressions for how efficient a specific heat pump can operate under cooling and heating demand and it is necessary to design heat exchangers based on SEER and SCOP. The actual weighting factor of the partial load operating condition is difficult to determine as it depends on the application and

Table 3
Seasonal cooling operating conditions.

Operating mode	Outdoor DB/WB temperature (°C)	Indoor DB/WB temperature (°C)	Air flow rate (m ³ /min)	Average face velocity(m/s)	Partial load ratio (%)
EER A	35/24	27/19	182	1.4	100
EER B	30/26	27/19	135	1	74
EER C	25/22	27/19	112	0.9	47
EER D	20/18	27/19	65	0.5	21

Notes: DB = dry bulb, WB = wet bulb

Table 4
Seasonal heating operating conditions.

Operating mode	Outdoor DB/WB temperature (°C)	Indoor DB/WB temperature (°C)	Air flow rate (m ³ /min)	Average face velocity (m/s)	Part load ratio (%)
COP A	-7/-8	20/15	149	1.1	88
COP B	2/1	20/15	135	1.0	54
COP C	7/6	20/15	86	0.7	35
COP D	12/11	20/15	65	0.5	15
TOL	-10/-11	20/15	182	1.4	-
Heating Standard	7/6	20/15	182	1.4	-

Notes: TOL = Temperature operating limit.

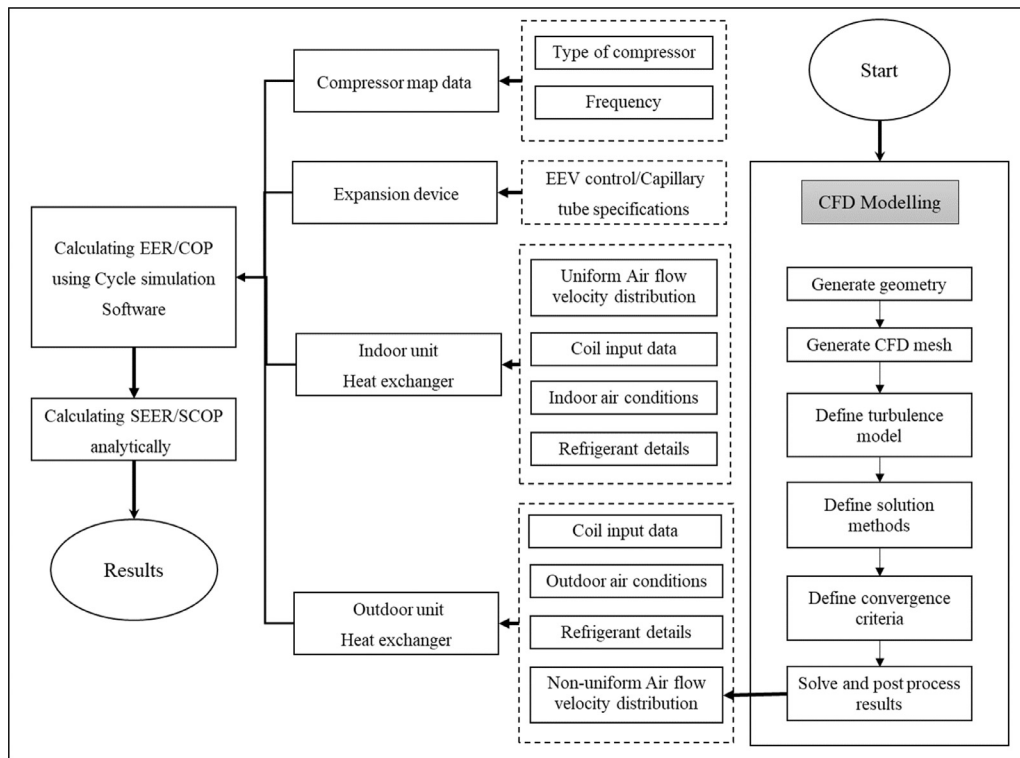


Fig. 5. Simulation model flow chart.

environmental conditions of the AC and heat pump system which can be expressed as Eqs. (13)–(18).

$$SEER = \frac{Q_c}{\frac{Q_c}{SEER_{on}} + H_{TO} \times P_{TO} + H_{SB} \times P_{SB} + H_{CK} \times P_{CK} + H_{OFF} \times P_{OFF}}, \quad (13)$$

where H is the number of hours in a year the heat pump is in stated operating mode (thermostat off mode, standby mode, crankcase heater mode, and off mode) and P is the energy consumption of the heat pump in corresponding mode. Q_c is defined as the reference annual cooling demand (kWh) and is expressed as Eq. (14).

$$Q_c = P_{design-c} \times H_{ce}, \quad (14)$$

where $P_{design-c}$ is the energy consumption in design operating mode, and H_{ce} is the number of annual operating hours. By accumulating cooling demand and electricity consumption for each temperature, $SEER_{on}$ can be calculated as the accumulated electricity consumption divided by the accumulated cooling demand as given by Eq. (15).

$$SEER_{on} = \frac{\sum_{j=1}^n h_j \cdot Pc(T_j)}{\sum_{j=1}^n h_j \cdot \left(\frac{Pc(T_j)}{EER_{PL}(T_j)} \right)}, \quad (15)$$

where T_j is the bin temperature, j is the bin number, n is the amount of bins, $Pc(T_j)$ is the cooling demand of the building for the corresponding temperature T_j , h_j is the number of bin hours occurring at the corresponding temperature T_j , and $EER_{PL}(T_j)$ is the EER

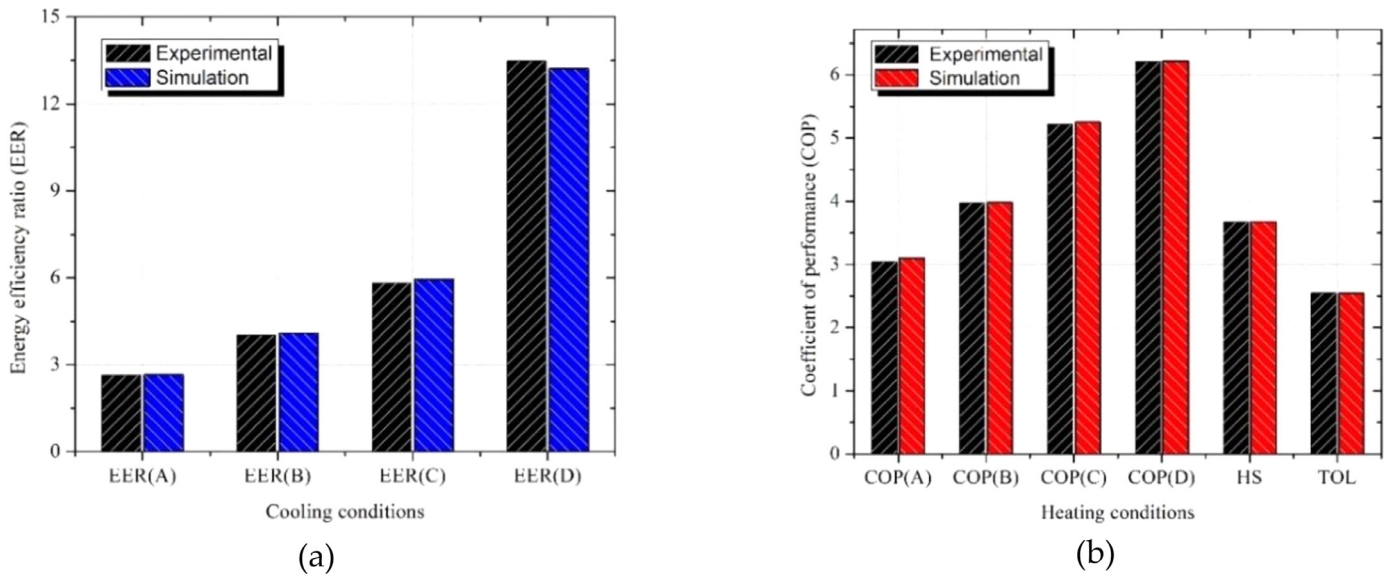


Fig. 6. (a) Energy efficiency ratio (EER) of the cycle; (b) Coefficient of performance (COP) of the cycle.

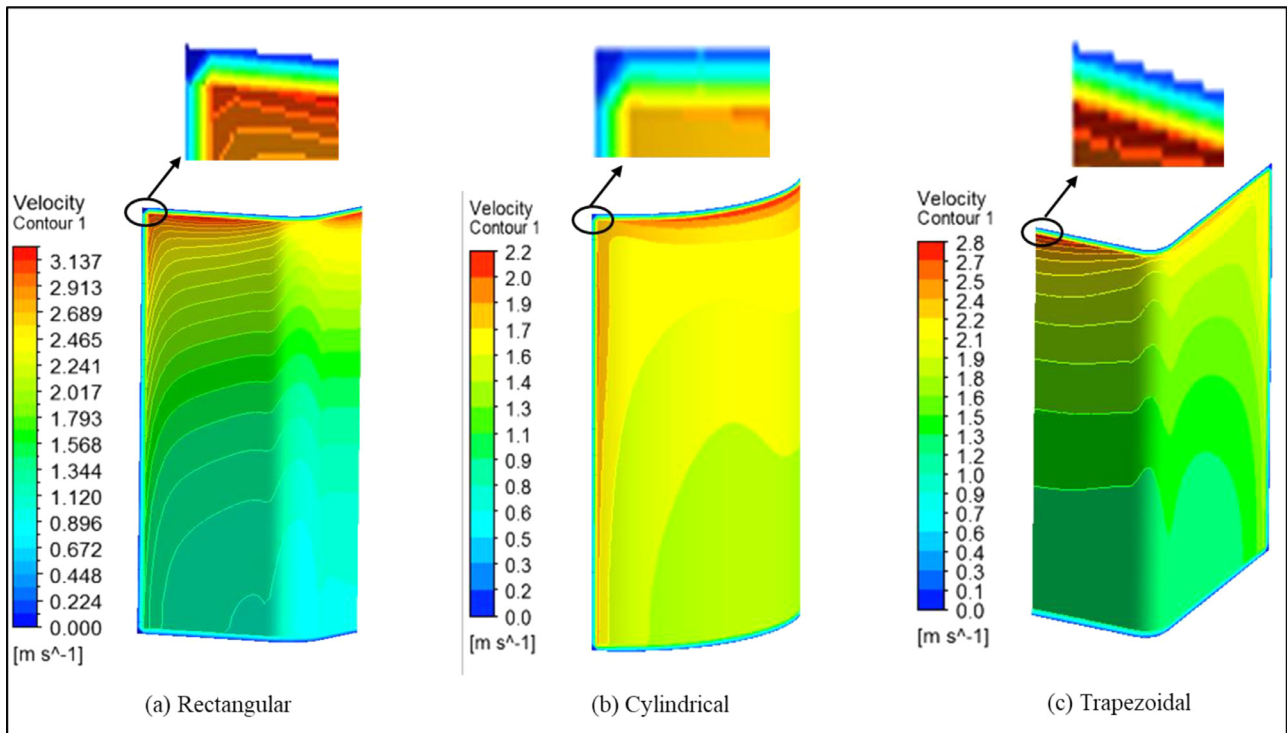


Fig. 7. Velocity contours for the three considered geometries.

values of the unit for the corresponding temperature T_j . Similarly, SCOP for heating case can be evaluated using Eqs. (16)–(18).

$$SCOP = \frac{Q_h}{\frac{Q_h}{SCOP_{on}} + H_{TO} \times P_{TO} + H_{SB} \times P_{SB} + H_{CK} \times P_{CK} + H_{OFF} \times P_{OFF}} \quad (16)$$

where

$$Q_h = P_{design-h} \times H_{he}, \quad (17)$$

$$SCOP_{on} = \frac{\sum_{j=1}^n h_j \cdot Ph(T_j)}{\sum_{j=1}^n h_j \cdot \left(\frac{Ph(T_j) - elbu(T_j)}{COP_{pl}(T_j)} + elbu(T_j) \right)} \quad (18)$$

where $Ph(T_j)$ is the heating demand of the building for the corresponding temperature T_j , $COP_{pl}(T_j)$ is the COP values of the unit for the corresponding temperature T_j , and $elbu(T_j)$ is the required capacity of an electric backup heater for the corresponding temperature T_j .

Alternatively, few standards are used nowadays, for better determination of the reflecting time of each load condition. One such method adopted in the current study is to utilize the weighting

factors of the European standard EN14825 [43] to calculate the average heat exchanger performance as given in Eqs. (19) and (20) for cooling and heating standards.

$$SEER = 0.03A + 0.33B + 0.41C + 0.23D \quad (19)$$

$$SCOP = 0.03A + 0.24B + 0.23C + 0.5D \quad (20)$$

where A, B, C, and D represent EER/COP under 100%, 75%, 50%, and 25% load conditions for cooling mode and 100%, 84%, 51%, and 33% load conditions for heating mode respectively. European standard EN14825 provides calculations method to evaluate the seasonal energy efficiency ratio (SEER) and seasonal coefficient of performance (SCOP). It specifies the outdoor and indoor operating conditions. The weighting coefficients are also fixed in accordance to the time of operating mode. Outdoor dry and wet bulb temperatures for four cooling cases during summer are 35/24, 30/26, 25/22, and 20/18 °C with comfortable indoor temperatures 27/19 °C. Corresponding winter temperatures for heating mode are -7/-8, 2/1, 7/6 and 12/11 °C with comfortable indoor temperatures 25/15 °C. Detail operating conditions are given in Tables 3 and 4. Fig. 5 shows the simulation flow chart to help clarify the numerical methodology.

3. Results and discussion

3.1. Model validation

Simulation results for EER and COP under rated as well as partial load operating conditions for the rectangular geometry have been compared with the available experimental data [44] as shown in Fig. 6. Numerical results were found to be in good agreement with experimental data having maximum percentage difference of 2.23% for EER and 1.97% for COP, respectively.

3.2. Air flow velocity contours

Eight cases were studied in total with condition EER(A) as the base case with rated volume flow 182 m³/min. Fig. 7(a)–(c) show velocity contours for the considered outdoor unit heat exchanger shapes. Velocity contours for the rectangular geometry are quite densely packed along the height of heat exchanger, whereas cylindrical geometry contours are widely spread and trapezoidal geometry lies between the two extremes. Wider spread velocity contours imply a more favorable velocity distribution due to smoother surface. Rectangular geometry has sharp 90° bends that cause flow separation and increase flow non-uniformity. Trapezoidal geometry bends are 110°, reducing separation and increasing flow uniformity.

Enlarged views in Fig. 7 indicate that airflow velocity suddenly drops to zero at the upper and lower ends for each geometry due to the heat exchanger ceiling, consistent with Lee et al. [21].

3.3. Face velocity profiles

Figs. 8–10 compare face airflow velocity distributions for each considered heat exchanger, respectively, where flow maps were generated from data sets compiled for sixty points along the height of each heat exchanger.

Fig. 8 shows the airflow velocity distribution for rectangular geometry under different seasonal conditions. Airflow velocity is quite non-uniform on the heat exchanger surface. The upper portion interacted with more air volume leading to higher air velocity decreasing gradually towards the lower part of the heat exchanger. This flow profile is consistent with Lee et al. [21] for multi-coil condenser. The gradual reduction in airflow velocity from top to bottom occurs due to the suction fan installed at the top of the heat exchanger.

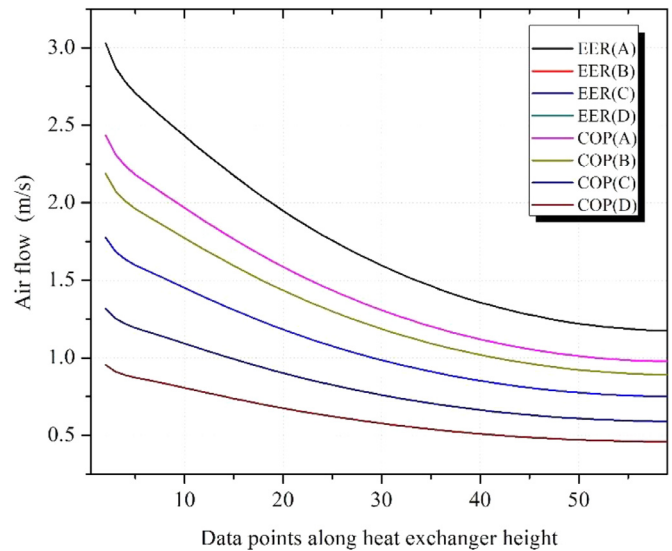


Fig. 8. Rectangular geometry airflow distribution.

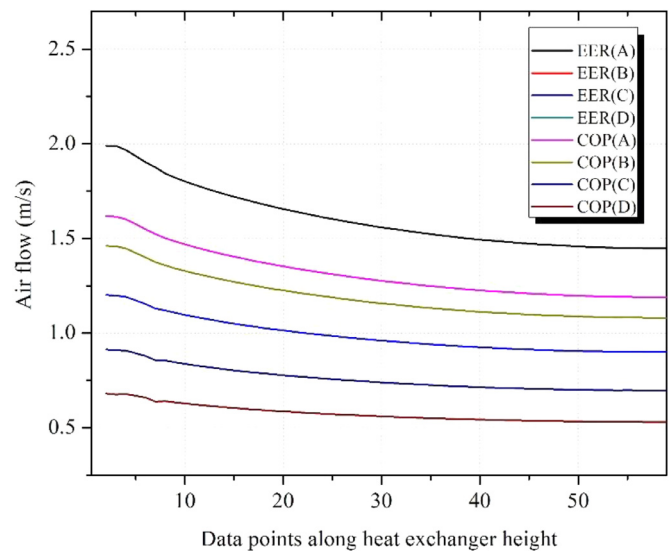


Fig. 9. Cylindrical geometry airflow distribution.

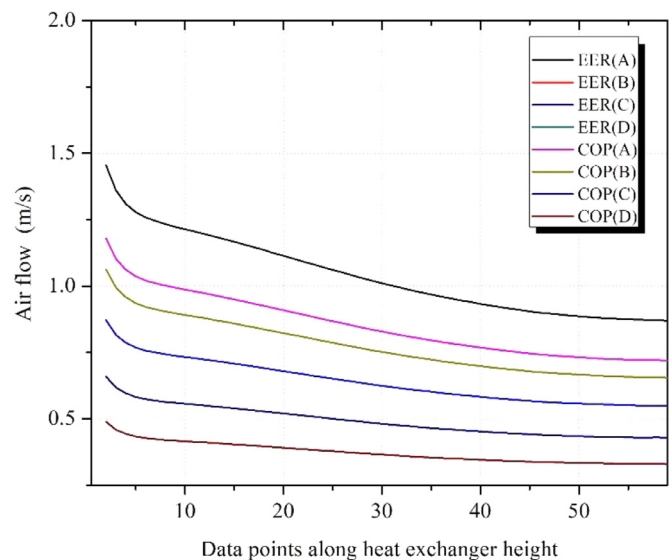


Fig. 10. Trapezoidal geometry airflow distribution.

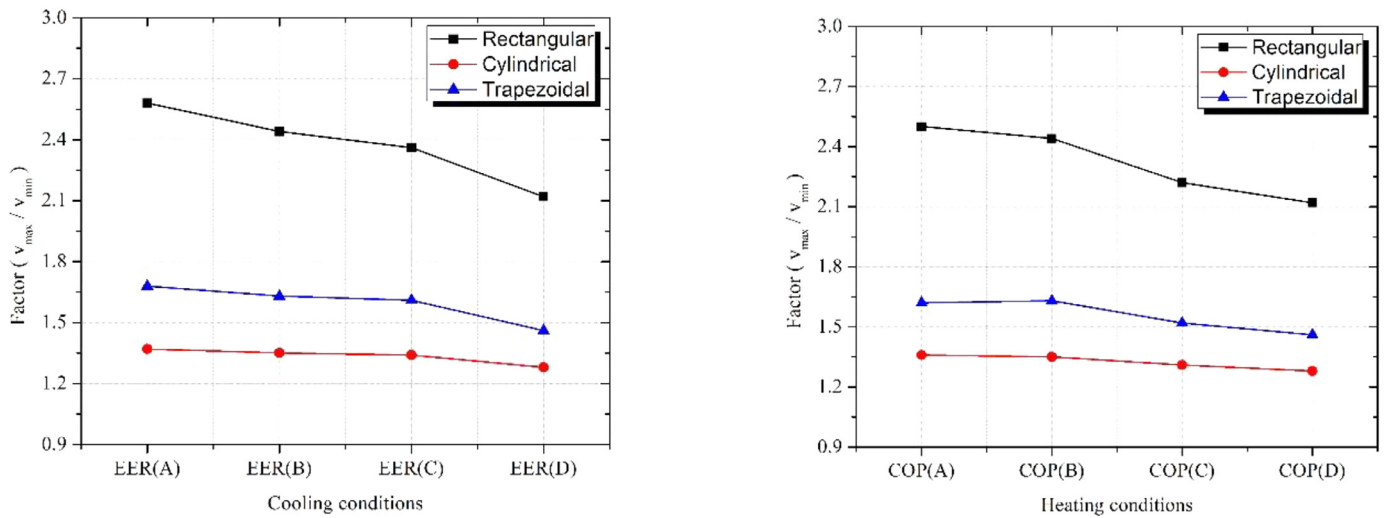


Fig. 11. Velocity variation for (a) cooling and (b) heating conditions.

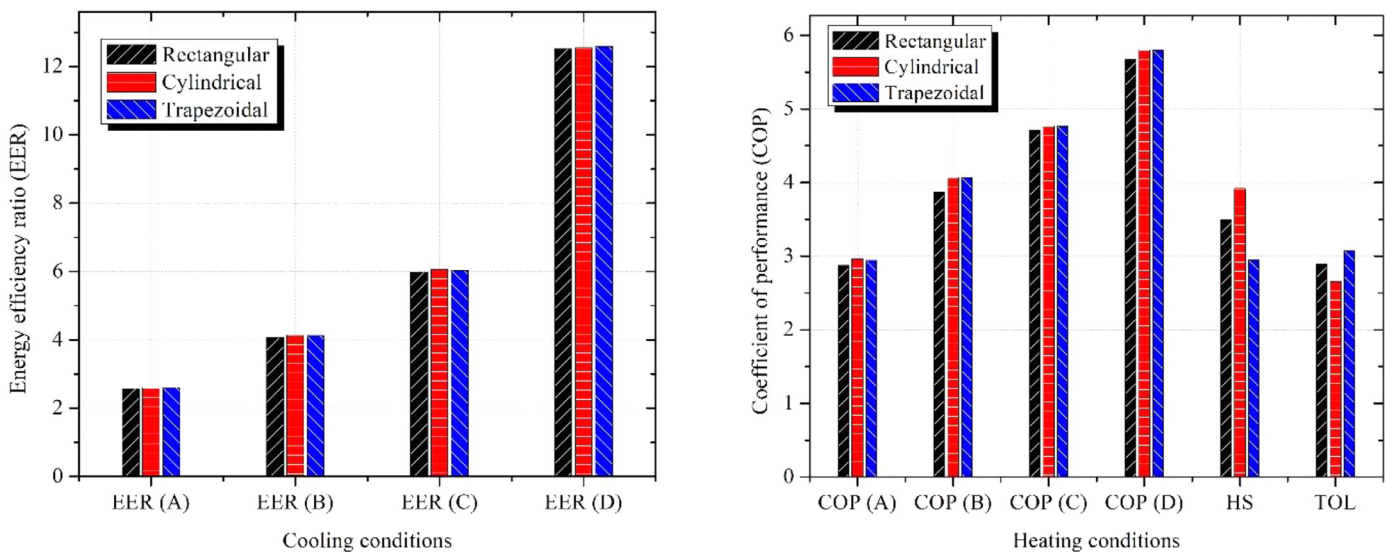


Fig. 12. Energy efficiency ratio (EER) and coefficient of performance (COP) for the considered outdoor geometries in (a) cooling, and (b) heating conditions.

Figs. 9 and 10 confirm that flow velocity distributions for cylindrical and trapezoidal geometries are more uniformly distributed compared to the rectangular geometry. This is because the cylindrical geometry has a smooth surface without abrupt bends, whereas trapezoidal geometry bends are less sharp than for the rectangular geometry.

Thus, velocity distribution is strongly affected by heat exchanger geometry, air filter blockage, fan position, etc. The results also suggest that outdoor air volume has a significant effect on velocity distribution, where increased outdoor air volume will increase flow distribution non-uniformity and vice versa.

Fig. 11(a) compares face velocity variation in terms of factors for rectangular, cylindrical and trapezoidal geometries under cooling conditions. The factor is defined as maximum face velocity divided by minimum value [45]. Face velocity variations from top to bottom for rectangular, cylindrical, and trapezoidal geometries were factor of 2.58 (3.02/1.17), 1.37 (1.98/1.44), and 1.68 (1.45/0.86) m/s under condition EER(A). Factors for other conditions were 2.44, 2.36, and 2.12; 1.35, 1.34, and 1.28; and 1.63, 1.61, and 1.46 for EER(B), EER(C) and EER(D) conditions for rectangular, cylindrical,

and trapezoidal geometries, respectively. Higher factors imply more non-uniform flow. Cylindrical geometry exhibits the lowest variation under all cooling conditions compared with rectangular and trapezoidal geometries, hence it has the least flow non-uniformity, due to surface smoothness.

Fig. 11(b) depicts factors for all three geometries under heating conditions. Similar to the cooling case (Fig. 11(a)), velocity variation confirms rectangular geometry produces the most non-uniform flow distribution due to abrupt bends, with trapezoidal more favorable, and cylindrical geometries the most favorable flow velocities.

3.4. Effect of outdoor heat exchanger shape on system performance

Calculated non-uniform airflow velocity distributions over the heat exchanger were subsequently used as an input for heat pump cycle calculations. Fig. 12 shows EER and COP under standard cooling and heating conditions for each geometric configuration, with average face velocities under cooling conditions 1.74, 1.28, 1.06, and 0.61 m/s; 1.61, 1.19, 0.98, and 0.57 m/s; and 1.03, 0.77, 0.64, and

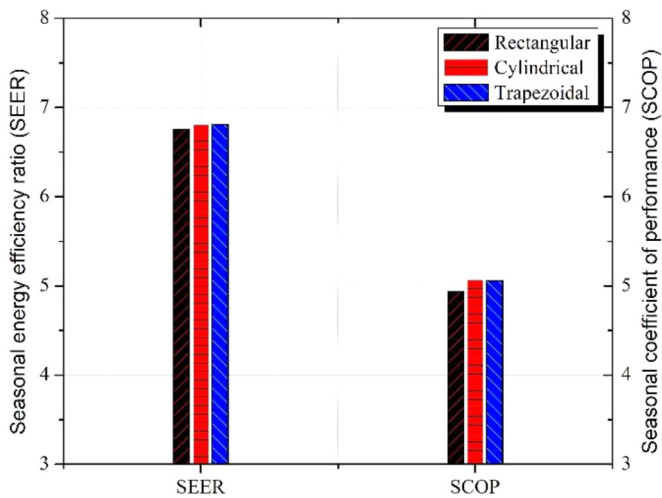


Fig. 13. Seasonal energy efficiency ratio (SEER) and seasonal coefficient of performance (SCOP) for the considered outdoor geometries.

0.37 m/s for rectangular, cylindrical and trapezoidal geometries, respectively. Average face velocities for rectangular geometry were 7–8% higher magnitude than cylindrical geometry. EER and COP should increase with increasing face velocity [5]. However, in this case, that deteriorates 2–5% in all conditions due to flow maldistribution.

Trapezoidal geometry has a more uniform flow velocity distribution than rectangular geometry, but its average face velocity is very low, which deteriorates overall system performance. Therefore, cylindrical geometry exhibits the best performance, with improved flow distribution uniformity without compromising much average face velocity magnitude.

3.5. Effect of outdoor heat exchanger shape on SEER/SCOP

SEER and SCOP are weighted formula enabling to take into account the variation of EER and COP for cooling and heating conditions of heat pump systems with the load ratio and the variation of air inlet condenser temperature. An efficient shape of outdoor unit with more favorable velocity distribution can maximize overall system's rated as well as part-load efficiency. Selecting the appropriately shaped design requires an understanding of the peak load operating points and the system's load profile in cooling and heating mode. To assess the seasonal performance variation of the heat pump system, SEER and SCOP are calculated according to Eqs. (19) and (20). The results are plotted for each outdoor unit shape as shown in Fig. 13. It can be seen from the results that cylindrical shape outdoor unit can enhance seasonal performance up to 3.70% due to more favorable velocity distribution. This improvement could provide significant energy savings throughout the year.

3.6. Effect of refrigerant circuits on SEER/SCOP

Although smart heat exchanger geometry can promote flow uniformity, non-uniform airflow distribution cannot be totally removed. The upper portion of the heat exchanger will still interact with more air volume compared to the lower part. Therefore, smart refrigerant circuit arrangement is essential to improve heat pump performance. Three circuit designs are investigated for each of the three outdoor heat exchanger geometries, as shown in Fig. 14. Circuit one has the symmetric number of passes on the upper and lower part of the heat exchanger, which is commonly found in heat exchangers. The second circuit design had 11 of 18 inlets set at the upper part of the heat exchanger and the remainder spread through the lower part. The third case reversed the second. There were 60 tubes in each heat exchanger row and 18 circuits in each heat exchanger.

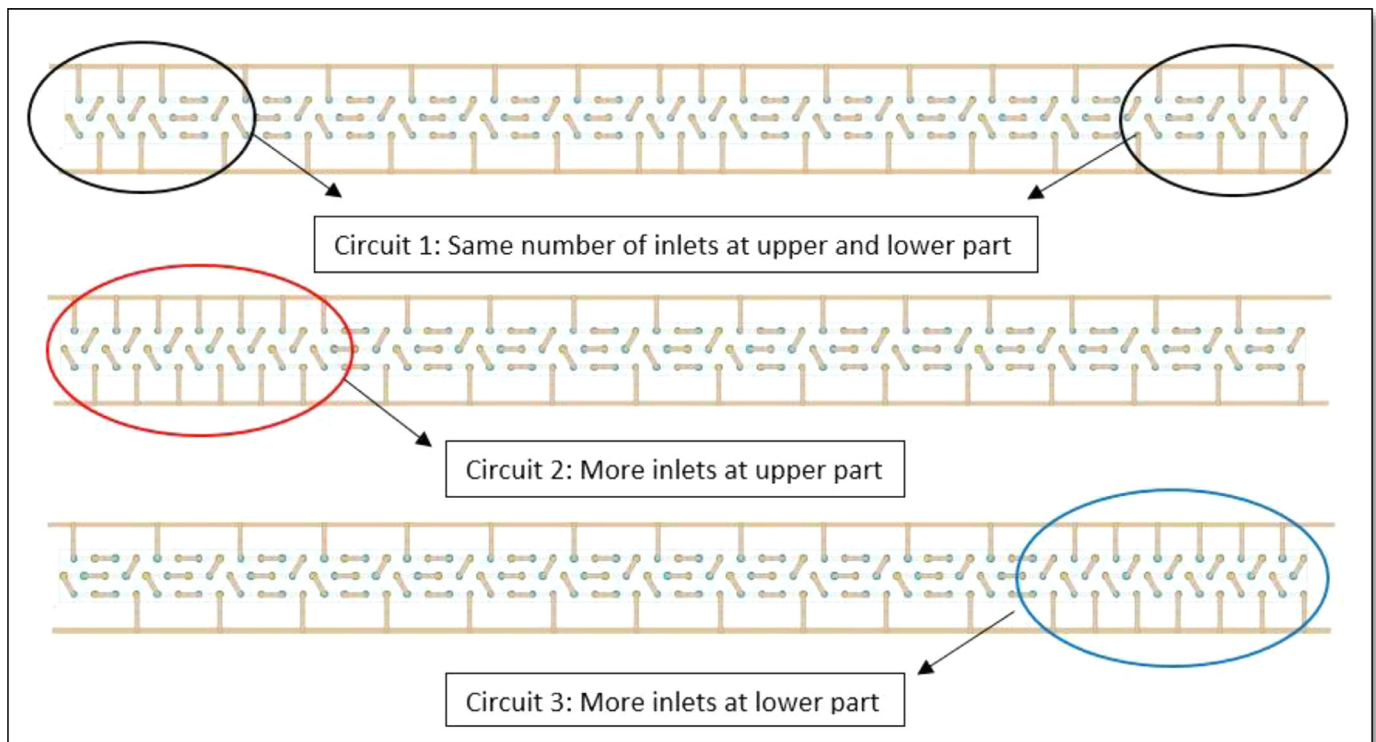


Fig. 14. The different refrigerant circuit arrangements considered.

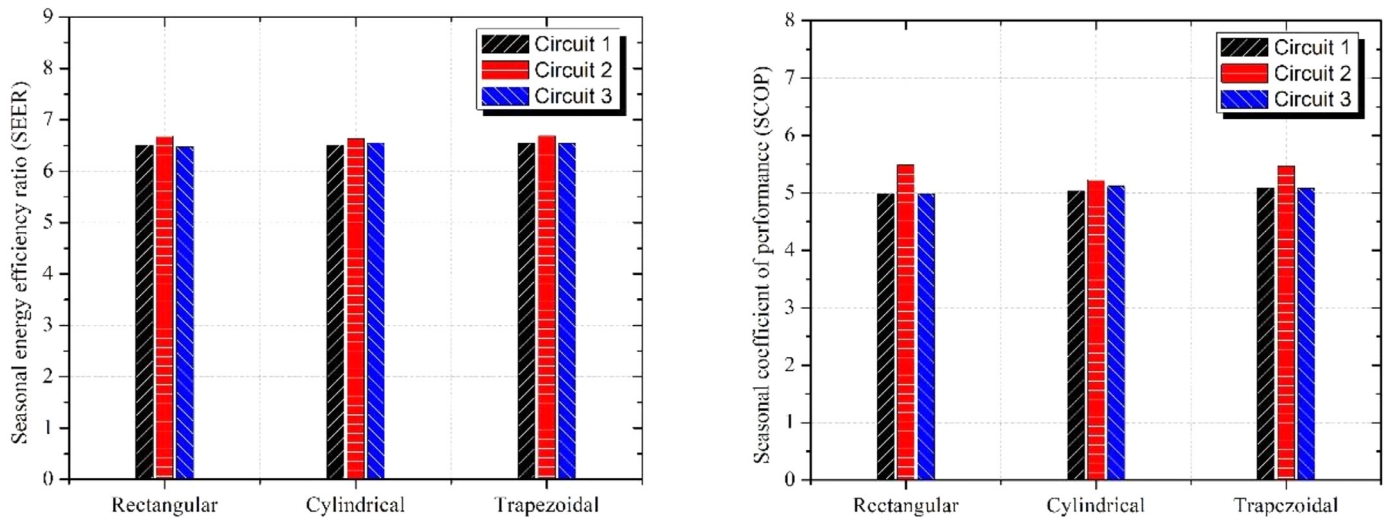


Fig. 15. (a) Seasonal energy efficiency ratio (SEER) and (b) seasonal coefficient of performance (SCOP) for three refrigerant circuit cases for the considered outdoor geometries.

Fig. 15 show circuit 2 improved SEER and SCOP by 3.25% and 9.97%, 1.20% and 2.27%, and 2.17% and 7.53% for rectangular, cylindrical, and trapezoidal geometry, respectively, compared with circuit 3. Since high air volume tends to occur in the upper part of the heat exchanger (Figs. 8–10), shorter circuits in the upper part causes higher refrigerant mass flow through those circuits, and hence more balanced air and refrigerant distribution, significantly improving heat transfer performance.

In contrast, performance deteriorated for all three geometries when more inlets were placed in the lower part of the heat exchanger, due to more unbalanced air and refrigerant distributions. Thus, smart heat exchanger refrigerant circuit arrangements are essential to address flow non-uniformity.

4. Conclusion

The current study presents the effect of outdoor unit heat exchanger shapes and refrigerant circuit designs on heat pump system performance improvement under partial load operating conditions. Computational fluid dynamics analysis has been used to find face velocity distribution for 10 different operating conditions, and cycle simulations are conducted to calculate SEER and SCOP. To find the effect of refrigerant pass on the system performance, we also investigated three heat exchanger refrigerant circuit layouts for each outdoor heat exchanger configuration. The following conclusions can be drawn.

- 1 Among the considered three heat exchanger configurations, maximum velocity variation was observed for rectangular geometry and minimum for cylindrical geometry under rated as well as partial load operating conditions. This implies cylindrical geometry performed well in all operating conditions compared to rectangular and trapezoidal shapes.
- 2 Average face velocity magnitudes were higher for rectangular geometry than cylindrical and trapezoidal geometries, especially under rated load conditions. It is worth finding that approximately 2–5% EER and COP enhancement were achieved for cylindrical compared to rectangular geometry even with low average face velocity. This implies that a more uniform distribution of flow velocity could enhance heat pump performance even by compromising face velocity magnitude to some extent.
- 3 The maximum seasonal performance improvement of 3.60% was achieved for cylindrical outdoor unit heat exchanger compared with rectangular geometry. This level of improvement could potentially save considerable energy annually.

- 4 The maximum SEER and SCOP improvements for rectangular (3.25% and 9.97%), cylindrical (1.20% and 2.27%), and trapezoidal (2.17% and 7.53%) geometries, respectively, were achieved by optimal refrigerant circuit arrangement relative to observed airflow distributions.

The current study has some limitations, in particular, the relatively small range of heat exchanger shapes and refrigerant circuit modifications. Further studies will extend the matrix by using an optimized fan design to generate more uniform airflow distribution, with balanced air and refrigerant mass flow rates to establish optimal refrigerant path.

Similar design criteria could also be applied to various heat exchangers used in commercial and industrial applications.

CRedit authorship contribution statement

Shehryar Ishaque: Formal analysis, Writing - original draft, Conceptualization. **Md Irfanul Haque Siddiqui:** Formal analysis, Writing - original draft. **Man-Hoe Kim:** Writing - review & editing, Supervision.

References

- [1] B. Metz, O.R. Davidson, P.R. Bosch, R. Dave LAM (Eds.), *Climate Change 2007: Mitigation. Contribution of Working Group III to the Fourth Assessment Report of the Inter- governmental Panel on Climate Change*, 2007.
- [2] M.-H. Kim, S.Y. Lee, S.S. Mehendale, R.L. Webb, Microchannel heat exchanger design for evaporator and condenser applications, *Adv. Heat Transf.* 37 (2003) 297–429.
- [3] A.A. Bhuiyan, A.K.M.S. Islam, Thermal and hydraulic performance of finned-tube heat exchangers under different flow ranges: A review on modeling and experiment, *Int. J. Heat Mass Transf.* 101 (2016) 38–59.
- [4] M.R. Kærn, W. Brix, B. Elmegaard, L.F.S. Larsen, Performance of residential air-conditioning systems with flow maldistribution in fin-and-tube evaporators, *Int. J. Refrig.* 34 (2011) 696–706.
- [5] W.J. Lee, J.H. Jeong, Heat transfer performance variations of condensers due to non-uniform air velocity distributions, *Int. J. Refrig.* 69 (2016) 85–95.
- [6] D.A. Yashar, H.H. Cho, P.A. Domanski, Measurement of air-velocity profiles for finned tube heat exchangers using particle image velocimetry, in: *12th International Refrig. Air-Conditioning Conference Purdue*, 2008, pp. 1–8.
- [7] A. Saleem, M.-H. Kim, Air-side thermal hydraulic performance of microchannel heat exchangers with different fin configurations, *Appl. Therm. Eng.* 125 (2017) 780–789.
- [8] A. Saleem, M.-H. Kim, CFD analysis on the air-side thermal-hydraulic performance of multi-louvered fin heat exchangers at low Reynolds numbers, *Energies* 10 (2017) 823.
- [9] C. T'Joën, M. De Paepe, F. Vanhee, Heat exchanger behavior in non uniform flow, *Exp. Heat Transf.* 19 (2006) 281–296.
- [10] J.M. Choi, W.V. Payne, P.A. Domanski, Effects of non-uniform refrigerant and air flow distributions on finned-tube evaporator performance, *International Conference Refrig.*, 2003.

- [11] X. Lu, X. Yu, Z. Qu, Q. Wang, T. Ma, Experimental investigation on thermoelectric generator with non-uniform hot-side heat exchanger for waste heat recovery, *Energy Convers. Manag.* 150 (2017) 403–414.
- [12] H. Peng, X. Ling, J. Li, Performance investigation of an innovative offset strip fin arrays in compact heat exchangers, *Energy Convers. Manag.* 80 (2014) 287–297.
- [13] P.R. Bobbili, B. Sunden, S.K. Das, An experimental investigation of the port flow maldistribution in small and large plate package heat exchangers, *Appl. Therm. Eng.* 26 (2006) 1919–1926.
- [14] E.B. Ratts, Investigation of flow maldistribution in a concentric-tube, counter-flow, laminar heat exchanger, *Heat Transf. Eng.* 19 (1998) 65–75.
- [15] C.S. An, D.H. Choi, Analysis of heat-transfer performance of cross-flow fin-tube heat exchangers under dry and wet conditions, *Int. J. Heat Mass Transf.* 55 (2012) 1496–1504.
- [16] P. Rao Bobbili, B. Sunden, S.K. Das, Thermal analysis of plate condensers in presence of flow maldistribution, *Int. J. Heat Mass Transf.* 49 (2006) 4966–4977.
- [17] X. Song, D. Huang, X. Liu, Q. Chen, Effect of non-uniform air velocity distribution on evaporator performance and its improvement on a residential air conditioner, *Appl. Therm. Eng.* 40 (2012) 284–293.
- [18] S.P. Datta, P.K. Das, S. Mukhopadhyay, Obstructed airflow through the condenser of an automotive air conditioner - effects on the condenser and the overall performance of the system, *Appl. Therm. Eng.* 70 (2014) 925–934.
- [19] M. Saeed, M.-H. Kim, Thermal-hydraulic analysis of sinusoidal fin-based printed circuit heat exchangers for supercritical CO₂ Brayton cycle, *Energy Convers. Manag.* 193 (2019) 124–139.
- [20] Z. Zhang, J. Yang, Y. Wang, A favorable face velocity distribution and a V-frame cell for power plant air-cooled condensers, *Appl. Therm. Eng.* 87 (2015) 1–9.
- [21] T.S. Lee, W.C. Wu, Y.K. Chuah, S.K. Wang, An improvement of airflow and heat transfer performance of multi-coil condensers by different coil configurations, *Int. J. Refrig.* 33 (2010) 1370–1376.
- [22] I.J. Kennedy, S.W.T. Spence, G.R. Spratt, J.M. Early, Investigation of heat exchanger inclination in forced-draught air-cooled heat exchangers, *Appl. Therm. Eng.* 54 (2013) 413–421.
- [23] J. Wen, Y. Li, S. Wang, A. Zhou, Experimental investigation of header configuration improvement in plate – fin heat exchanger, *Appl. Therm. Eng.* 27 (2007) 1761–1770.
- [24] C. Butler, R. Grimes, The effect of wind on the optimal design and performance of a modular air-cooled condenser for a concentrated solar power plant, *Energy* 68 (2014) 886–895.
- [25] X. Peng, Z. Liu, J.T. Chan Qiu, Effect-of-inlet-flow-maldistribution-on-the-passage-arrangement-design-of-multi-stream-plate-fin-heat-exchanger, *Appl. Therm. Eng. J.* 103 (2016) 67–76.
- [26] N. Ploskas, C. Laughman, A.U. Raghunathan, N.V. Sahinidis, Optimization of circuitry arrangements for heat exchangers using derivative-free optimization, *Chem. Res. Des.* 131 (2018) 16–28.
- [27] M. Kim, K. Lee, S. Song, Effects of pass arrangement and optimization of design parameters on the thermal performance of a multi-pass heat exchanger, *Int. J. Heat Fluid Flow* 29 (2008) 352–363.
- [28] C.K. Bach, E.A. Groll, J.E. Braun, W.T. Horton, Mitigation of air flow maldistribution in evaporators, *Appl. Therm. Eng.* 73 (2014) 877–885.
- [29] J. Liu, W. Wei, G. Ding, C. Zhang, M. Fukaya, K. Wang, et al., A general steady state mathematical model for fin-and-tube heat exchanger based on graph theory, *Int. J. Refrig.* 27 (2004) 965–973.
- [30] D.A. Yashar, J. Wojtusiak, K. Kaufman, P.A. Domanski, A dual-mode evolutionary algorithm for designing optimized refrigerant circuitries for finned-tube heat exchangers, *HVAC&R Res.* 18 (2012) 834–844.
- [31] B. Lu, J. Wu, Z. Liang, C. Liu, Circuitry arrangement optimization for multi-tube phase change material heat exchanger using genetic algorithm coupled with numerical simulation, *Energy Convers. Manag.* 175 (2018) 213–226.
- [32] R.S. Nagaosa, Turbulence model-free approach for predictions of air flow dynamics and heat transfer in a fin-and-tube exchanger, *Energy Convers. Manag.* 142 (2017) 414–425.
- [33] P.A. Domanski, D. Yashar, Application of an evolution program for refrigerant circuitry optimization, ACRECONF 2007, “Challenges To Sustainability”, New Delhi, India, December 7–8 2007.
- [34] J. Kim, T. Sibilli, M.Y. Ha, K. Kim, S.Y. Yoon, Compound porous media model for simulation of flat top U-tube compact heat exchanger, *Int. J. Heat and Mass Transf.* 138 (2019) 1029–1041.
- [35] ANSYS FLUENT, FLUENT user’s guide release 16.0 2015.
- [36] C.S. An, M.-H. Kim, Thermo-hydraulic analysis of multi-row cross-flow heat exchangers, *Int. J. Heat Mass Transf.* 120 (2018) 534–539.
- [37] Traviss D.P., Baron A.B., Rohsenow W.M., Forced-Convection condensation inside tubes, 1971.
- [38] J.O. Hinze, *Turbulence*, 2nd Ed, McGraw-Hill Publishing Co, New York, 1975.
- [39] Domanski P.A. An evaporator simulation model accounting for refrigerant and one-dimensional air distribution, 1989.
- [40] J.H. Lee, S.W. Bae, K.H. Bang, M.H. Kim, Experimental and numerical research on condenser performance for R-22 and R-407C refrigerants, *Int. J. Refrig.* 25 (2002) 372–382.
- [41] M.-H. Kim, A study on the performance of a split system inverter air-conditioner at different operation conditions, *Trans. KSME (B)* 22 (1998) 113–121.
- [42] C.I. Graham, *Whole Building Design Guide*, a program of the National Institute of Building Sciences, Viridian Energy & Environmental, Inc., a Vidaris, Inc. company, 2016 <http://www.wbdg.org/resources/hvac.php>.
- [43] European Standard EN14825, Air conditioners, liquid chilling packages and heat pumps, with electrically driven compressors, for space heating and cooling - Testing and rating at part load conditions and calculation of seasonal performance (2018).
- [44] K.J. Kim, Private Communication of Samsung Electronics Co. Ltd., 2018.
- [45] D.A. Yashar, S. Lee, P.A. Domanski, Rooftop air-conditioning unit performance improvement using refrigerant circuitry optimization, *Appl. Therm. Eng.* 83 (2015) 81–87.